ISSN 0021-8944, Journal of Applied Mechanics and Technical Physics, 2022, Vol. 63, No. 6, pp. 923–930. © Pleiades Publishing, Ltd., 2022.
Russian Text © A.L. Kupershtokh, D.A. Medvedev.

PERFORATION OF THIN LIQUID FILMS UNDER THE ACTION OF A NONUNIFORM ELECTRIC FIELD

A. L. Kupershtokh[a,*] **and D. A. Medvedev**[a]

UDC 532.64+536.42+532.2

Abstract: A non-stationary electrohydrodynamic model has been developed to describe the behavior of a dielectric liquid film on the electrode surface in the surrounding gas. It has been shown that the application of a nonuniform electric field can lead to perforation of the film with the formation of new contact lines. Field nonuniformity was produced using a round insulating insert at the center of the lower electrode. The perforation process is determined by the electric field strength, film thickness, the radius of the non-conductive insert, and the contact angle between the liquid and the solid substrate.

Keywords: lattice Boltzmann method, dynamics of multiphase media, liquid dielectrics, electric field, computer simulation, parallel computations on graphics accelerators.

DOI: 10.1134/S0021894422060025

INTRODUCTION

Efficient cooling of hot surfaces is very important in microfluidic and microelectronic devices. One cooling method is based on producing thin films or many evaporating liquid droplets placed on a solid surface with three-phase contact lines [1, 2]. It has been shown theoretically and experimentally [3, 4] that for droplets on a substrate surface, the heat transfer process is closely related to the enhancement of liquid evaporation near the contact lines. Thus, creating new contact lines by perforating liquid films is a promising method for improving the cooling efficiency.

Many experimental, theoretical, and computer simulation studies have been devoted to the behavior of droplets [5–13], bubbles [14, 15], and liquid films [13, 16] in an electric field. Electric field was also used for manipulation of droplets [7, 13]. The action of an electric field on dielectric droplets can enhance heat transfer from a solid substrate [8]. However, numerical studies of the perforation of dielectric films in an electric field are almost absent. Computer models of this process should take into account surface tension and electrical and gravitational forces.

In a previous study [13], we have shown the fundamental possibility of rupturing liquid films by the action of an nonuniform electric field and numerically investigated the process of generating contact lines by perforating thin films of a dielectric liquid on an electrode surface taking into account the properties of the wetted surface. The nonuniform field was produced at the boundaries of an insulating disk inserted flush into the hole in a flat electrode. The lower flat electrode was electrically grounded. When a high voltage is applied to the upper flat electrode, the dielectric liquid is pulled into the regions of the stronger electric field at the edges of the insert. In this case, depending on the geometry and field strength, rupture of the liquid film can occur, resulting in the formation of new contact lines. In the present work, we performed a three-dimensional computer simulation of this process.

[a]Lavrent'ev Institute of Hydrodynamics, Siberian Branch, Russian Academy of Sciences, Novosibirsk, 630090 Russia; *skn@hydro.nsc.ru, dmedv@hydro.nsc.ru. Translated from Prikladnaya Mekhanika i Tekhnicheskaya Fizika, Vol. 63, No. 6, pp. 13–20, November–December, 2022. Original article submitted June 15, 2022; revision submitted June 15, 2022; accepted for publication July 25, 2022.

*Corresponding author.

The dimensionless parameters that determine the behavior of the films are the Bond number Bo and the electric Bond number Bo_E.

For the three-dimensional simulation of non-stationary two-phase hydrodynamics, we used the lattice Boltzmann equation method (LBE, LBM) [17–19], which takes into account surface tension at the liquid–vapor interface, gravitational and electrostatic forces, and the interaction of the liquid with the solid substrate. The electric and hydrodynamic equations of the three-dimensional problem are solved simultaneously. The distribution of the electric field strength in the region between the flat electrodes was calculated numerically at each time step by solving the Poisson equation for the electric field potential.

Compute unified device architecture (CUDA) technology was used for parallel programming on a multi-core graphics processor unit (GPU).

LATTICE BOLTZMANN METHOD

In the lattice Boltzmann method, liquid flows are simulated as the dynamics of an ensemble of pseudoparticles (single-particle distribution functions f_k) that can move along the links of a regular spatial lattice. The pseudoparticle velocities $\boldsymbol{c}_k$ can have a limited set of values. In the 19-velocity D3Q19 model [20] used in this study, these values are 0, $h/\Delta t$ and $\sqrt{2}\,h/\Delta t$ (h is the lattice step, and Δt is the time step). The corresponding lattice vectors are $\boldsymbol{e}_k = \boldsymbol{c}_k\,\Delta t$. The evolution of the single-particle distribution functions f_k is described by the equation

$$f_k(\boldsymbol{x} + \boldsymbol{c}_k\,\Delta t, t + \Delta t) = f_k(\boldsymbol{x}, t) + \Omega_k\{f_k\} + \Delta f_k.$$

The collision operator Ω_k is taken in the form of the Bhatnagar–Gross–Krook collision operator (relaxation of distribution functions to local equilibrium) [20]

$$\Omega_k(f_k(\boldsymbol{x}, t)) = \frac{f_k^{eq}(\rho, \boldsymbol{u}) - f_k(\boldsymbol{x}, t)}{\tau}.$$

The dimensionless relaxation time τ determines the kinematic viscosity of the liquid $\nu = (\tau - 1/2)\theta\,\Delta t$, where $\theta = (h/\Delta t)^2/3$ is the kinetic temperature of LBE pseudoparticles. The equilibrium distribution functions $f_k^{eq}(\rho, \boldsymbol{u})$ are taken in the form of an expansion of the Maxwell distribution in powers of the liquid mass velocity $\boldsymbol{u}$ up to the second order [21]:

$$f_k^{eq}(\rho, \boldsymbol{u}) = \rho w_k\Big(1 + \frac{(\boldsymbol{c}_k \cdot \boldsymbol{u})}{\theta} + \frac{(\boldsymbol{c}_k \cdot \boldsymbol{u})^2}{2\theta^2} - \frac{\boldsymbol{u}^2}{2\theta}\Big).$$

The density ρ and velocity of the liquid $\boldsymbol{u}$ are calculated as the first two moments of the distribution functions

$$\rho = \sum_{k=0}^{18} f_k, \qquad \rho\boldsymbol{u} = \sum_{k=1}^{18} \boldsymbol{c}_k f_k.$$

The weight coefficients for the three-dimensional 19-velocity D3Q19 model are $w_0 = 1/3$, $w_{1-6} = 1/18$, and $w_{7-18} = 1/36$ [20].

Changes in the distribution functions Δf_k due to the action of body (internal, gravitational, and electrostatic) forces are calculated using the exact difference method (EDM) [19, 22]

$$\Delta f_k = f_k^{eq}(\rho, \boldsymbol{u} + \Delta\boldsymbol{u}) - f_k^{eq}(\rho, \boldsymbol{u}),$$

where $\Delta\boldsymbol{u} = \boldsymbol{F}\Delta t/\rho$ is the change in velocity over one time step.

The internal forces between the material at neighboring nodes of the liquid are introduced to simulate phase transitions in the LBE method. The total force acting on a node is expressed in terms of the gradient of the pseudopotential $U = P(\rho, T) - \rho\theta$ [23]:

$$\boldsymbol{F}_{in}(\boldsymbol{x}) = -\nabla U \tag{1}$$

($P(\rho, T)$ is the equation of state of the liquid, and T is the temperature). It has previously been proposed to introduce a special function $\Phi = \sqrt{-U}$. Using this function, formula (1) can be rewritten for the total force in mathematically equivalent form [18, 24]:

$$\boldsymbol{F}(\boldsymbol{x}) = 2A\,\nabla(\Phi^2) + (1 - 2A)2\Phi\,\nabla\Phi. \tag{2}$$

Here A is a free parameter which is chosen so as to provide the best fit of the liquid–vapor coexistence curve to the given equation of state of the liquid. In the present work, we used the van der Waals equation of state in reduced

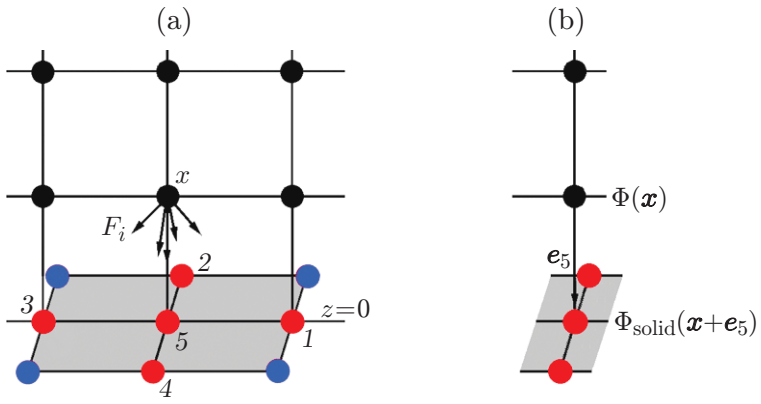

Fig. 1. Interaction forces of the liquid with the solid surface (a) and values of the function $\Phi_{solid}(\boldsymbol{x}+\boldsymbol{e}_5)=\Phi(\boldsymbol{x})$ on the solid surface (b): (*1*–*5*) are the node numbers.

variables, for which the optimal value is $A=-0.152$ [18, 24]. Equation (2) allows us to write an approximation of the pseudopotential gradient in a combined finite difference form with improved isotropy [18, 24]. At a reduced temperature $T/T_{\text{cr}}=0.6$, the surface tension at the interfaces $\sigma=5.1$ LBM units (T_{cr} is the critical temperature).

It should be noted that in the second order of the Chapman–Enskog expansion, the LBE equations lead to the macroscopic equations of hydrodynamics [22, 25], i.e., the well-known continuity and Navier–Stokes equations. This can serve as a justification for the LBE method.

GEOMETRY AND BOUNDARY CONDITIONS

The calculations were performed in a rectangular domain with dimensions $L_,L_y$, and L_z. In the x and y directions, periodic boundary conditions were used. The impermeability and no-slip boundary conditions on the lower and upper solid boundaries $z=0$ and $z=L_z$ in the LBE method were set using the "bounce-back" rule [26].

The wettability of the electrodes was simulated using a model in which the interaction forces between a node $\boldsymbol{x}$ of the liquid and the nearest five nodes on the solid surface are introduced (Fig. 1a) [15]:

$$\boldsymbol{F}(\boldsymbol{x})=B\Phi(\boldsymbol{x})\sum_{j=1}^{5}w(\boldsymbol{e}_j)\Phi_{solid}(\boldsymbol{x}+\boldsymbol{e}_j)\cdot\boldsymbol{e}_j.$$

At each node of the solid surface, the function Φ_{solid} takes the same value as at the node of the liquid located directly above them $\boldsymbol{x}$ (Fig. 1b), i.e., $\Phi_{solid}(\boldsymbol{x}+\boldsymbol{e}_5)=\Phi(\boldsymbol{x})$. The wettability of the solid surface is defined by the parameter B [15]. In the range of angles $\beta=60$–130°, the dependence of the static contact angle on the parameter B is approximately linear: $\beta=90^\circ-520^\circ\,(B-1)$ (Fig. 2). For $B=1$, the static contact angle is $\beta=90^\circ$ (neutral wettability). Values $B>1$ correspond to the wetted surface (for $B=1.06$, the contact angle is $\beta\approx60^\circ$), and values $B<1$ correspond to the case of poor wettability (for $B=0.92$, $\beta\approx130^\circ$).

CALCULATION OF ELECTRICAL FORCES

The electrostatic force acting on the dielectric liquid is given by the Helmholtz formula [27]

$$\boldsymbol{F}=-\frac{\varepsilon_0E^2}{2}\nabla\varepsilon+\frac{\varepsilon_0}{2}\nabla\Big[E^2\rho\Big(\frac{\partial\varepsilon}{\partial\rho}\Big)_T\Big],$$

where E is the local electric field strength, ε_0 is the permittivity of vacuum, and ε is the permittivity of the liquid. For nonpolar dielectric liquids, the dependence $\varepsilon(\rho)$ is calculated using the Clausius–Mossotti formula

$$\varepsilon(\rho)=1+\frac{3\alpha\rho}{1-\alpha\rho}.$$

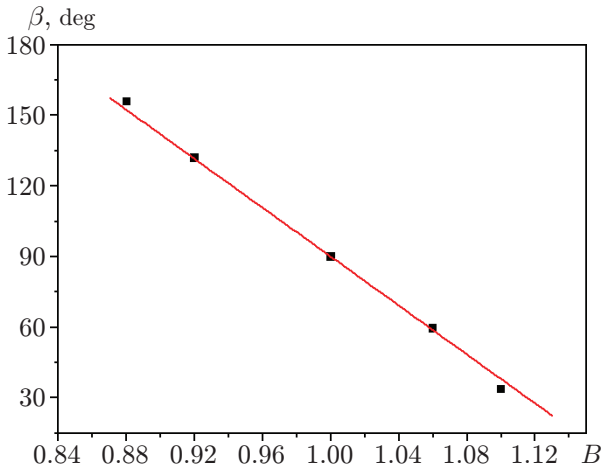

Fig. 2. Dependence of the contact angle β on the parameter B for $T/T_{\rm cr} = 0.6$.

Thus, during the deformation process, the permittivity $\varepsilon(\rho)$ of the liquid varies in time and space. The parameter $\alpha = 0.215$ was determined in such a way that the permittivity of the liquid was $\varepsilon_l = 4$ for a value of the reduced density of the liquid dielectric used in the simulation $\tilde{\rho}_l = 2.31$. (The value $\varepsilon \approx 1$ corresponds to the permittivity of vapor.)

The distribution of the electric field potential φ between the electrodes with a change in the shape of the film was calculated at each time step by solving the Poisson equation

$$\nabla \cdot (\varepsilon_0 \varepsilon \nabla \varphi) = 0. \tag{3}$$

The changes in the permittivity distribution in space and time were taken into account. In the x and y directions, periodic boundary conditions for the potential were used. A pulse of constant voltage V was applied to the electrodes. In this case, the potential of the upper electrode is $\varphi(x, y, L_z) = V$ (Fig. 3). The lower electrode is electrically grounded: $\varphi(x, y, 0) = 0$. On the surface of the non-conductive insert in the lower electrode, the boundary conditions $\partial\varphi/\partial z = 0$ were used. Equation (3) was solved at each time step by simple iterations. The electric field strength was then calculated by the formula $\boldsymbol{E} = -\nabla\varphi$.

To provide the specified initial electric field strength E_0 above the film surface, the applied voltage was calculated as follows:

$$V = E_0(L_z - \delta(1 - 1/\varepsilon_l))$$

(δ is the film thickness).

COMPUTER SIMULATION RESULTS

Parallel calculations were performed using all cores of the Titan-V graphics processor unit (GPU) (internal memory 12 Gb, 5120 cores). For the three-dimensional LBM simulation of the dynamics of dielectric films, the GPU internal memory can accommodate three-dimensional lattices with a size of up to $560 \times 560 \times 144$ (approximately $45{\cdot}10^6$ nodes). In this work, the computation performance was more than $130{\cdot}10^6$ node updates per second (NUPS)).

Figure 3 shows the process of perforating a thin film with permittivity ε_l after applying voltage between horizontal electrodes. Field inhomogeneity was produced using a round insulating insert *1* with radius R_0 located at the center of the lower electrode.

After a high voltage is applied, the dielectric liquid is pulled into the regions of increased electric field near the edges of the insert. Depending on the film thickness, the film may rupture, resulting in the formation of a new contact line (see Figs. 3a and 3d). Then the liquid continues to move not only due to the action of electrostatic forces, but also due to inertia (see Figs. 3c and 3f).

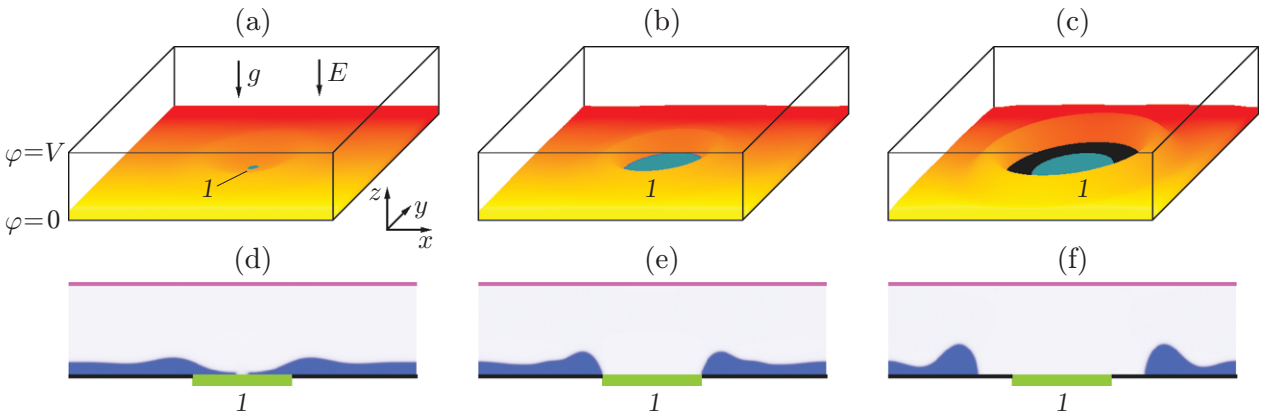

Fig. 3. Perforation of a liquid dielectric film after the application of the electric field (a–c) and the liquid density distribution in the central vertical section (d–f) for $\beta = 90°$, $\delta = 20$, $R_0 = 80$, $\varepsilon_l = 4$, $\mathrm{Bo} = 0.018$, $\mathrm{Bo}_E = 1.18$, and $\mathrm{Bo}_E^* = 18.9$ (computational lattice size $560 \times 560 \times 144$) at different times: (a, d) $t = 3900$ LBM units, (b, e) $t = 5600$ LBM units, (c, f) $t = 8400$ LBM units; *1*) round non-conductive insert in the lower electrode.

Table 1. Time to liquid film rupture at a constant thickness of this film

R_0	Bo_E^*	t
20	1.71	11 400
30	3.84	6700
40	6.82	4400
60	15.30	3200
80	27.30	3400
100	42.60	4000
150	96.00	5700

Table 2. Time to start of liquid film rupture at a constant radius of the insert $R_0 = 40$

δ	Bo_E	Bo_E^*	t
20	1.71	6.82	4400
30	2.56	4.55	5800
40	3.41	3.41	7500
50	4.27	2.73	9400
60	5.12	2.27	11 000

A dimensionless parameter that determines the behavior of liquid droplets in a purely gravitational field is the Bond number $\mathrm{Bo} = \rho g R^2/\sigma$, where R is the characteristic droplet size. It is obvious that the degree of deformation of dielectric liquid droplets increases with increasing electric field. It is common to use the electric Bond number $\mathrm{Bo}_E = \varepsilon_0(\varepsilon_l - 1)E_0^2 R/(\varepsilon_l \sigma)$. At the same time, for the process of perforation of dielectric films, the use of the similar definition $\mathrm{Bo}_E = \varepsilon_0(\varepsilon_l - 1)E_0^2\delta/(\varepsilon_l\sigma)$ leads to contradictions. However, the calculation results show that for parameter values $\delta = 20$, $\varepsilon_l = 4$, $\sigma = 5.1$, $\tau = 0.58$, $B = 1$, and $\beta = 90°$, i.e., for a constant value $\mathrm{Bo}_E = 1.71$, the time to the start of perforation (in LBM units) depends strongly on the radius of the non-conductive insert R_0 in the lower electrode (Table 1).

At $R_0 \leqslant 60$, the time to film rupture decreases with increasing radius of the insert. At $R_0 \geqslant 80$, film perforation occurs later than at $R_0 = 60$ (see Table 1). This may be due to the fact that film rupture starts along a circle, and not at the center of the insert (Fig. 4), i.e., the rupture mechanism changes and the perforation process slows down. Furthermore, a liquid droplet remains above the center of the insert, i.e., a more complex hydrodynamic process occurs.

In addition, a series of calculations was carried out for a constant radius of the insulating insert $R_0 = 40$. With increasing film thickness δ, the time to its rupture t increased (Table 2), and the Bond electric number Bo_E also increased, but should decrease. Therefore, in this case, it is proposed to use a modified definition of the electric Bond number depending on the film thickness δ and on the radius of the insulating insert R_0:

$$\mathrm{Bo}_E^* = \varepsilon_0(\varepsilon_l - 1)E_0^2 R_0^2/(\delta\varepsilon_l\sigma).$$

This definition provides an adequate qualitative evaluation of the process of perforation of liquid dielectric films, at least in the case of film rupture at the center of the insert without droplet formation.

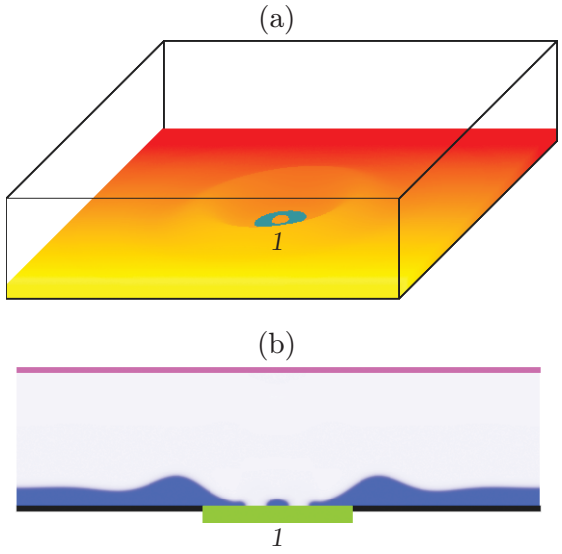

Fig. 4. Process of film perforation with the formation of a droplet (a) and the liquid density distribution in the central vertical section (b) for $t = 3400$ LBM units, $\delta = 20$, $R_0 = 80$, $\varepsilon_l = 4$, Bo $= 0.018$, and $\mathrm{Bo}_E^* = 27.3$ ($560 \times 560 \times 144$ computational lattice): (*1*) round non-conductive insert in the lower electrode).

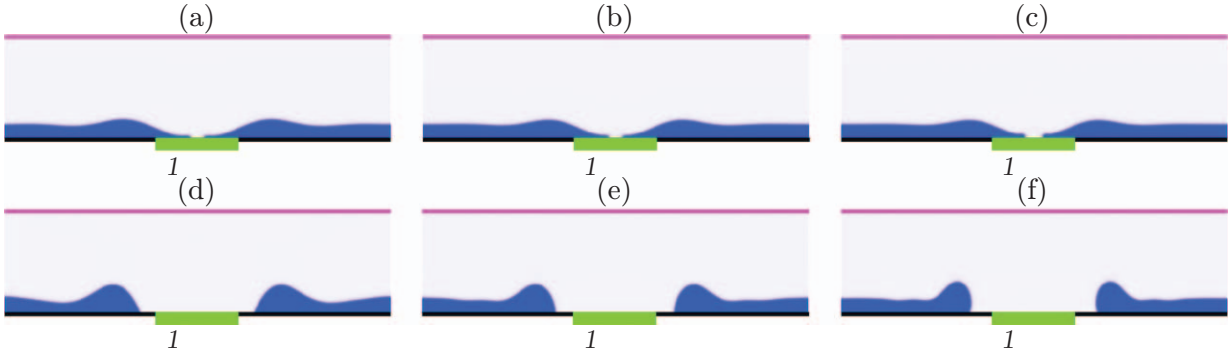

Fig. 5. Liquid density distribution in the central section for $\delta = 20$, $R_0 = 60$, $\varepsilon_l = 4$, Bo $= 0.018$, $\mathrm{Bo}_E^* = 12.9$, different contact angles, and different times: (a, d) $\beta = 60°$, (b, e) $\beta = 90°$, (c, f) $\beta = 130°$; (a) $t = 4800$ LBM units, (b) $t = 3500$ LBM units, (c) $t = 3200$ LBM units, (d) $t = 8200$ LBM units, (e) $t = 5800$ LBM units, (f) $t = 5000$ LBM units; (*1*) round non-conductive insert in the lower electrode.

For realistic values of the physical parameters $\delta = 2$ mm, $R_0 = 8$ mm, $\varepsilon_l = 7$, $\sigma = 0.073$ N/m, and an electric field strength $E_0 = 10$ kV/cm, the modified electric Bond number is $\mathrm{Bo}_E^* = 3.33$.

Figure 5 shows the effect of surface wettability on the film perforation process. For β =60, 90, and 130°, the time to film rupture was 4800, 3500, and 3200 LBM units. The time to start of perforation decreases with decreasing surface wettability.

CONCLUSIONS

The perforation of dielectric liquid films on the solid surface of an electrode containing a round non-conductive insert has been studied by three-dimensional simulation using the lattice Boltzmann method. At a constant electric

field strength, the time to perforation increases with increasing film thickness and depends significantly on the insert radius. For moderate values of the radius of the insert, the time to perforation can be evaluated qualitatively using a modified Bond electric number that takes into account both factors. In the case of large insert radii, the formation of a droplet above the center of the insert is observed during perforation. In this case, the time to the start of perforation increases, and the dependence of the time on the insert radius changes fundamentally. On surfaces with lower wettability (large contact angle), the perforation process develops faster than on surfaces with neutral or high wettability.

Thus, it has been shown that dielectric liquid films can be perforated using a pulsed electric field. Obviously, more than one hole can be produced in the film. This leads to the formation of new contact lines, resulting in increased heat transfer from the substrate.

This work was supported by the Russian Science Foundation (Grant No. 22-29-01055).

REFERENCES

1. M. Potash and P. C. Wayner, "Evaporation from a Two-Dimensional Extended Meniscus," Intern. J. Heat Mass Transfer **15** (10), 1851–1863 (1972).
2. P. C. Wayner "A Dimensionless Number for the Contact Line Evaporative Heat Sink," J. Heat Transfer **111** (3), 813–815 (1989).
3. A. L. Karchevsky, I. V. Marchuk, and O. A. Kabov, "Calculation of the Heat Flux Near the Liquid-Gas-Solid Contact Line," Appl. Math. Modell. **40** (2), 1029–1037 (2016).
4. V. S. Ajaev and O. A. Kabov, "Heat and Mass Transfer near Contact Lines on Heated Surfaces," Intern. J. Heat Mass Transfer **108**, 918–932 (2017).
5. G. Taylor "Disintegration of Water Drops in an Electric Field," Proc. Roy. soc. London. Ser. A . Math. Phys. Sci. **280** (1382), 383–397 (1964).
6. A. M. Imano and A. Beroual, "Deformation of Water Droplets on Solid Surface in Electric Field," J. Colloid Interface Sci. **298** (2), 869–879 (2006).
7. Y. Liu, K. Oh, J. G. Bai, et al. "Manipulation of Nanoparticles and Biomolecules by Electric Field and Surface Tension," Comput . MethodsAppl. Mech. Engng. **197** (25–28), 2156–2172 (2008).
8. V. Vancauwenberghe, P. Di Marco, and D. Brutin, "Wetting and Evaporation of a Sessile Drop under an External Electrical Field: A Review," Colloids Surfaces. A. Physicochem. Engng Aspects. **432**, 50–56 (2013).
9. L. T. Corson, C. Tsakonas, B. R. Duffy, et al., "Deformation of a Nearly Hemispherical Conducting Drop Due to an Electric Field: Theory and Experiment," Phys. Fluids **26** (12), 122106 (2014).
10. L. T. Corson, N. J. Mottram, B . R. Duffy, and S. K. Wilson, "Dynamic Response of a Thin Sessile Drop of Conductive Liquid to an Abruptly Applied or Removed Electric Field," Phys. Rev. E **94** (4), 43112 (2016).
11. M. J. Gibbons, C. M. Howe, P. Di Marco, and A. J. Robinson, "Local Heat Transfer to an Evaporating Sessile Droplet in an Electric Field," J. Phys. Conf. Ser. **745** (3), 32066 (2016).
12. M. Akbari and S. Mortazavi, "Three-Dimensional Numerical Simulation of Deformation of a Single Drop under Uniform Electric Field," J. Appl. Fluid Mech. **10** (2), 693–702 (2017).
13. D. A. Medvedev and A. L. Kupershtokh, "Electric Control of Dielectric Droplets and Films," Phys. Fluids **33** (12). 122103 (2021).
14. Y. Wang, D. Sun, A. Zhang, and B. Yu, "Numerical Simulations of Bubble Dynamics in the Gravitational and Uniform Electric Fields," Numer. Heat Transfer. Pt A. Applications **71** (10), 1034–1051 (2017).
15. A. L. Kupershtokh and D. A. Medvedev, "Dynamics of Bubbles in Liquid Dielectrics under the Action of an Electric Field: Lattice Boltzmann Method," J. Phys. Conf. Ser. **1359**, 12116 (2019).
16. N. Zubarev, "Self-Similar Solutions for Conic Cusps Formation at the Surface of Dielectric Liquids in Electric Field," Phys. Rev. E **65**, 055301(R) (2002).
17. X. Shan and H. Chen, "Lattice Boltzmann Model for Simulating Flows with Multiple Phases and Components," Phys. Rev. E **47** (3), 1815–1819 (1993).
18. A. L. Kupershtokh, D. A. Medvedev, and D. I. Karpov, "On Equations of State in a Lattice Boltzmann Method," Comput. Math. Appl. **58** (5), 965–974 (2009).
19. A. L. Kupershtokh, "Criterion of Numerical Instability of Liquid State in LBE Simulations," Comput. Math. Appl. **59** (7), 2236–2245 (2010).

20. Y. H. Qian, D. d'Humières, and P. Lallemand, "Lattice BGK Models for Navier–Stokes Equation," Europhys. Lett. **17** (6), 479–484 (1992).
21. J. M. V. A. Koelman, "A Simple Lattice Boltzmann Scheme for Navier–Stokes Fluid Flow," Europhys. Lett. **15** (6), 603–607 (1991).
22. A. L. Kupershtokh, "Accounting for Body Forces in Lattice Boltzmann Equations," Vestn. Novosib. Gos. Univ. Ser. Mat., Mekh. Inform. **4** (2), 75–96 (2004).
23. Y. H. Qian and S. Chen, "Finite Size Effect in Lattice-BGK Models," Intern. J. Modern Phys. C **8** (4), 763–771 (1997).
24. A. L. Kupershtokh, "Simulation of Flows with Liquid–Vapor Interfaces Using the Lattice Boltzmann method," Vestn. Novosib. Gos. Univ. Ser. Mat., Mekh. Inform **5** (3), 29–42 (2005).
25. S. Chen and G. D. Doolen, "Lattice Boltzmann Method for Fluid Flow," Annual Rev. Fluid Mech. **30**, 329–364 (1998).
26. J. Hardy, O. de Pazzis, and Y. Pomeau, "Molecular Dynamics of a Classical Lattice Gas: Transport Properties and Time Correlation Functions," Phys. Rev. A **13** (5), 1949–1961 (1976).
27. L. D. Landau and E. M. Lifshitz, *Electrodynamics of Continuous Media* (Nauka, Moscow, 1982) [in Russian].